ON THE INTENSITY OF SATURN LIGHTNING

G. Fischer[*], W. Macher[*], M. D. Desch[†], M. L. Kaiser[†], P. Zarka[‡],
W. S. Kurth[§], W. Farrell[†], A. Lecacheux[‡], B. Cecconi[§],
and D. A. Gurnett[§]

Abstract

In the year 2004 the radio signatures of most SEDs (Saturn Electrostatic Discharges) were recorded when Cassini was at a distance of more than 80 Saturn radii away from the planet, and their intensities were generally just a few dB above the galactic background. SEDs were recorded by the Cassini RPWS (Radio and Plasma Wave Science) instrument in a frequency range of 1–16 MHz, in which the electric antenna resonance is located, and hence, the antenna properties are highly frequency dependent. We calculate absolute intensities for the SEDs taking into account the frequency dependence of the effective antenna length vectors, which are calculated by wire–grid modelling of the spacecraft. We find an average source power of 50 W/Hz of all SEDs recorded in 2004, and a slight fall–off of the power spectrum with $f^{-0.5}$ for frequencies f from 4 to 16 MHz.

1 Lightning on Saturn

SEDs are believed to be the radio signature of lightning discharges in Saturn's atmosphere, and their study is one of the main scientific objectives of the RPWS instrument [Gurnett et al., 2004]. Throughout this paper we still use the term "SED" for Saturn's lightning flashes, which was introduced when the nature of this bursts was still unclear or misinterpreted (Evans et al. [1982], ring source). As all the energy of a lightning flash stems from the electrostatic energy of oppositely charged clouds, it still seems to be appropriate to use "Saturn Electrostatic Discharge" also with the current atmospheric storm source explanation.

In 2004 more than 5300 flashes attributed to lightning in Saturn's atmosphere were detected by the RPWS instrument. The flashes were organized in episodes recurring repeatedly with Saturn's rotation, and there is also a clustering of episodes which we call

---

[*] *Space Research Institute, Austrian Academy of Sciences, Schmiedlstrasse 6, A-8042 Graz, Austria*
[†] *NASA Goddard Space Flight Center, Greenbelt, MD, USA*
[‡] *Observatoire de Paris, LESIA, UMR CNRS 8109, 92195 Meudon, France*
[§] *Dept. of Physics and Astronomy, University of Iowa, Iowa City, IA 52242, USA*

an SED storm. There were three storm systems after Cassini SOI (Saturn Orbit Insertion), which are called A, B, and C storm, occurring in mid–July, first half of August, and throughout most of September 2004, respectively [Gurnett et al., 2005]. Additionally there was also one storm system about one month before SOI at the end of May 2004, now called the 0 (zero) storm [Fischer et al., 2006; Desch et al., 2005]. As the spacecraft (s/c) was quite far away from Saturn (more than 80 Saturn radii for storm A, and around 300 Saturn radii for storm 0), the measured intensities were just a few dB above the galactic background. When the Voyagers flew by Saturn in the early 1980s the presence of the SEDs was interpreted as lightning discharges from an equatorial storm system, and there was a clear fall–off of intensities with distance from Saturn with maximum intensities up to 30 dB above background around closest approach. The average source powers of the flashes were calculated by Zarka and Pedersen [1983] to be around 100 W/Hz and 10 W/Hz for Voyager 1 and 2, respectively. They also calculated a true spectrum for the SEDs, where it turned out that the spectral power is practically constant with frequency f from 5 to 26 MHz. Obtaining the true spectrum is important with regard to the nature of the discharge: A relatively flat spectrum suggests that the initiating discharge must be very fast. A typical negative cloud–to–ground lightning return stroke on Earth has a spectral energy density peak around 10 kHz and decreases with f^{-2} up to about 5 MHz, and then there is a spectral "knee" with a decrease of f^{-4} to f^{-5} at higher frequencies [Rakov and Uman, 2003]. In this work we will calculate the absolute intensities and the true spectrum of all Saturnian lightning discharges recorded by Cassini/RPWS in 2004.
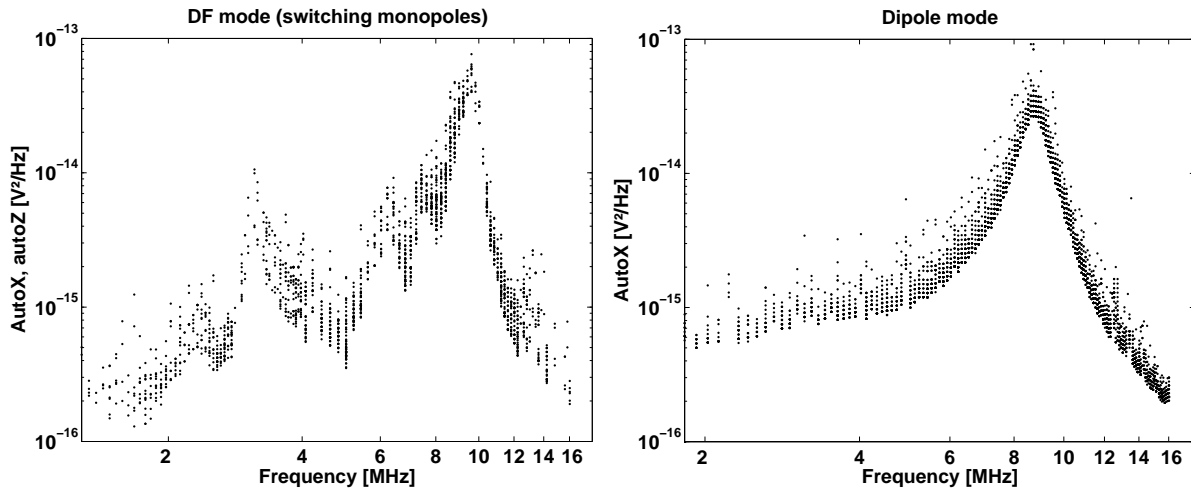

Figure 1: Left side: Strength of measured SED signals (in V^2/Hz) as a function of frequency in the direction–finding (DF) mode with switching monopoles. Right side: The same as on the left but with the HFR (High Frequency Receiver) being in the dipole mode. The monopole signal is the autocorrelation of the u or the v–antenna signal (the stronger one is taken) against the s/c–body, and the x–dipole signal is the autocorrelation of the voltages between the u and v–antenna. In the DF mode also the autocorrelations of the w–antenna are measured and plotted in the left panel (two antenna signals per SED event).

Figure 1 shows the strength of all antenna signals (in V^2/Hz) of all SEDs measured by RPWS as a function of frequency for two different receiver modes. It can be seen that in the frequency range from 1 to 16 MHz the signal strength varies over 2 magnitudes from
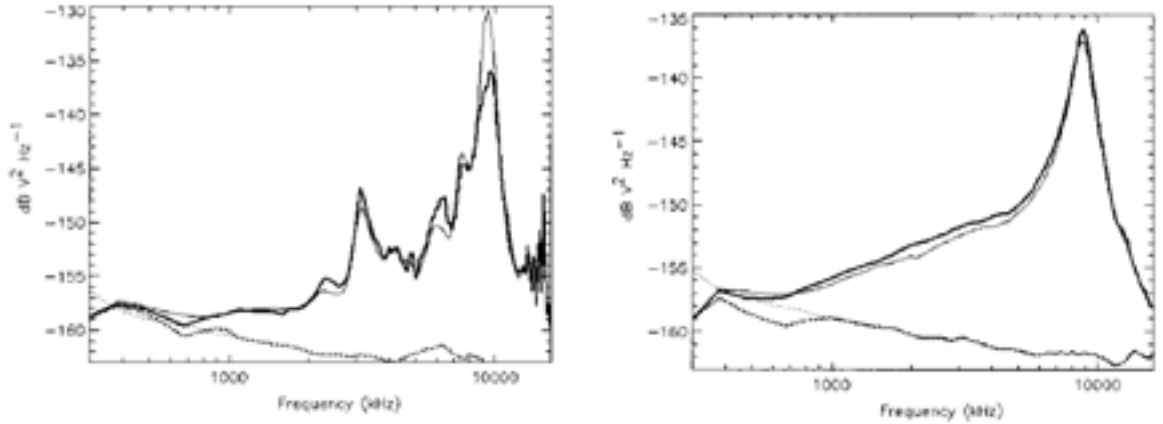
Figure 2: Left side: Galactic background noise spectrum (plus receiver noise) measured by the HFR with the monopole antennas. The main electrical resonance is around 9.5 MHz, and the peaks around 3 and 13 MHz are probably due to interference. The boldface continuous curve is an average background during a 6 months interval, the lightface curve was obtained at another shorter time interval close to Jupiter, and the dotted curves are receiver noise levels. Right side: The same as on the left but measured in the dipole mode. Here the resonance is around 8.8 MHz (both from Zarka et al. [2004]).

about 10^{-15} to 10^{-13} V^2/Hz. Due to the large gain at the antenna resonances at 9.5 MHz for the monopole and at 8.8 MHz for the dipole the SED signals as well as the background are pronounced near these frequencies. Lightning flashes from the SED storms A and B were recorded when the instrument was in the DF mode, and the intensities of these flashes are plotted in the left panel of Figure 1, whereas during the storms 0 and C the instrument was in the dipole mode, and the respective flashes are plotted in the right panel. Figure 1 can be compared very well with Figure 2 taken from Zarka et al. [2004], where the galactic background is drawn as a function of frequency. It is evident that most SED signals are grouped just a few dB above the background, and as the galactic background does not vary considerably in the frequency range from 2 to 16 MHz according to the model of Dulk et al. [2001], we can conclude that there should be no significant variation of the spectral power within this frequency range, which will also be shown in section 4.

2   Effective antenna length vectors of RPWS antennas

For the description of an antenna on a spacecraft the so–called effective antenna length vector $\vec{h}_{eff}$ (vector effectus longitudinis) is an appropriate tool. It has been used for the RPWS antenna system onboard Cassini to describe the properties of the three monopole antennas u, v, w, and the x–dipole between u and v (Vogl et al. [2004], Cecconi and Zarka [2005]). With wire–grid modelling [Fischer et al., 2001] this vector is calculated by

integrating the surface current density $\vec{J}_F$ (A/m) over the s/c–surface F [Macher, 1997]:

$$\vec{h}_{eff} = \frac{1}{I} \oint \vec{J}_F(\vec{r}) e^{-i\vec{k}\vec{r}} dF \approx \frac{1}{I} \sum_{wires} \int I_l(\vec{r}) e^{-i\vec{k}\vec{r}} \vec{dl} \tag{1}$$

with I as the current at the feed point, $\vec{k}$ as the wave vector, $\vec{r}$ as the coordinates of antenna elements, and dF as the surface area element. Wire–grid modelling is a numerical simulation method where an antenna system is represented by a suitable wire–grid modell. As a s/c normally has conducting surfaces, a wire–grid of the whole s/c including the antennas has to be constructed. The currents on the wires are calculated by an electromagnetic code, which numerically solves the underlying boundary value problem of the electric integral equation by the method of moments. Finally, $\vec{h}_{eff}$ is calculated with equation (1) by summing up all integrals over all wires of the current I_l along a wire with the infinitesimal line element $\vec{dl}$. For wavelengths exceeding the dimensions of the s/c the imaginary part of the effective antenna length vector can be neglected (by setting $e^{-i\vec{k}\vec{r}} = 1$, i.e. quasistatic frequency range). For the RPWS antenna system onboard Cassini this is a valid approximation for frequencies $f < 2$ MHz. The respective effective length vectors in the quasistatic frequency range for all RPWS antennas were determined by the experimental rheometry method [Rucker et al., 1996], by wire–grid modelling [Fischer et al., 2001], and by in–flight calibration as listed in Vogl et al. [2004]. As most SEDs have higher frequencies, we have to make use of equation (1) and calculate complex antenna length vectors, to derive the absolute intensities of the SEDs. It is important to note that the base capacitances for the electric antennas have to be included in the modelling to give correct results for the antenna lengths. We used the base capacitances $C_u = 118.9$ pF, $C_v = 113.1$ pF, $C_w = 105.7$ pF for the three antennas u, v, w, respectively, which were taken from Gurnett et al. [2004].

3   How to get absolute intensities

For the calculation of the incident flux of the SEDs we do not use the galactic background as a reference spectrum, but we try a different approach via a theoretical modelling of the s/c with the RPWS antenna system. To obtain the incident flux in $V^2/(m^2$ Hz) we just divide the measured antenna signal given in $V^2/$Hz by a "reception area" in m^2. This area is identical to the square of the projection of the effective length vector $|\vec{h}_p|^2$ into the wave plane. (This "reception area" is not identical to the so–called effective area of an antenna, which is defined over the ratio of the available power at the terminals of the antenna to the power density of an incident polarization–matched plane wave [Collin and Zucker, 1969].) The wave plane is the plane perpendicular to the incident wave, hence we have to know the direction of incidence to calculate $\vec{h}_p$. Additionally in the frequency range of interest, which is not the quasistatic regime anymore, the effective length vector itself depends on the frequency and the direction of the incoming wave, and hence has to be calculated for every frequency and direction separately (see Figure 3, where $|\vec{h}_p|$ is displayed as a function of frequency at all those times when SEDs occur). We assume that the SEDs stem from Saturn, so we know the direction of the incoming wave in the

s/c fixed coordinate system of Cassini from the attitude data. Additionally we have to assume that the SEDs are unpolarized (Stokes parameters $Q = U = V = 0$), which is a reasonable assumption according to Zarka and Pedersen [1983]. The basic mathematical formula for our calculation is the following:

$$\langle V_n V_n^* \rangle = \frac{1}{2} |\vec{h}_p|^2 \langle |\vec{E}|^2 \rangle = \langle S_{Flux} \rangle Z_0 |\vec{h}_p|^2 \tag{2}$$

with $\langle V_n V_n^* \rangle$ as the measured autocorrelation from the n–th antenna in V^2/Hz, $\vec{h}_p$ as the projection of the effective length vector into the wave plane (in m), $\vec{E}$ as the wave electric field (in V/m), $\langle S_{Flux} \rangle$ being the incident power flux in W/(m^2 Hz), Z_0 as the impedance of free space with $Z_0 = 120\pi$ Ω, and the brackets $\langle\ \rangle$ denote time–averaging operations. The second identity of equation (2) is obtained by inserting the identity $\langle S_{Flux} \rangle = \frac{1}{2Z_0} \langle |\vec{E}|^2 \rangle$. In the quasistatic frequency range equation (2) can be derived from
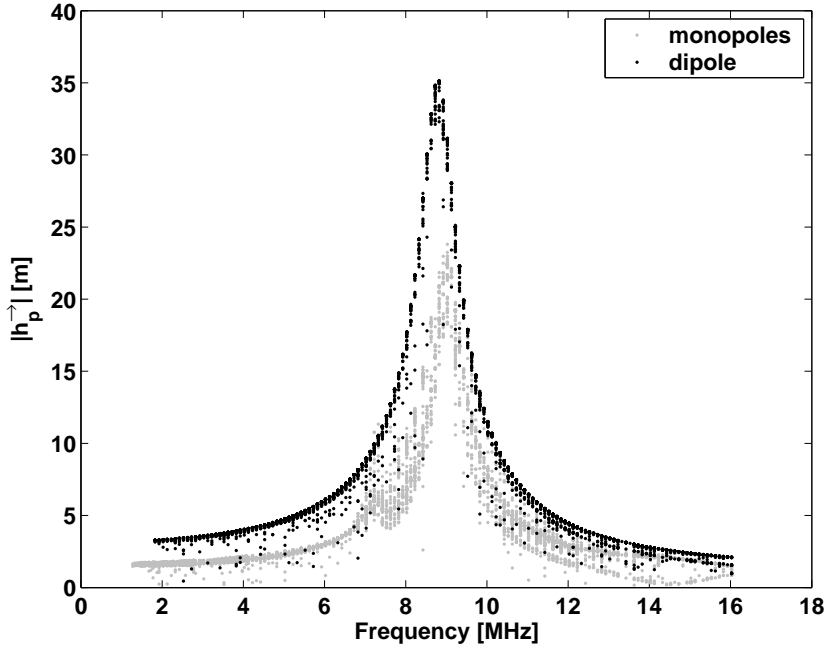

Figure 3: *Magnitude of the projection of the effective length vector $|\vec{h}_p|$ into the wave plane as a function of frequency. $|\vec{h}_p|$ is calculated by wire–grid modelling for the various positions of Saturn at the times when SED signals occur.*

the following equation used for direction–finding:

$$\langle V_n V_n^* \rangle = \frac{S_{Stokes} h_n^2}{2} (\Omega_n^2 + \Psi_n^2), \tag{3}$$

which is taken from equations (1) to (3) from Cecconi and Zarka [2005] by setting $Q = U = V = 0$, as we assume unpolarized waves. The index n denotes one of the three monopole antennas u, v, w or the x–dipole, and h_n is the effective length of the respective antenna. The Stokes parameter S_{Stokes} is given by the sum of the squares of the components of

the electric field vector $\vec{E}$ in the wave plane spanned by the unit vectors $\vec{e}_1$ and $\vec{e}_2$: $S_{Stokes} = \langle|\vec{e}_1\vec{E}|^2 + |\vec{e}_2\vec{E}|^2\rangle$, and finally $\Omega_n = (\vec{h}_n\vec{e}_1)/h_n$ and $\Psi_n = (\vec{h}_n\vec{e}_2)/h_n$ are the coordinates of the n–th antenna unit vector projected on the wave plane. Inserting the last three identities into equation (3) leads directly to

$$\langle V_n V_n^* \rangle = \frac{1}{2}\langle|\vec{e}_1\vec{E}|^2 + |\vec{e}_2\vec{E}|^2\rangle[(\vec{h}_n\vec{e}_1)^2 + (\vec{h}_n\vec{e}_2)^2] = \frac{1}{2}|\vec{h}_p|^2\langle|\vec{E}|^2\rangle, \tag{4}$$

as $\vec{h}_p = (\vec{h}_n\vec{e}_1, \vec{h}_n\vec{e}_2, 0)$ and $\vec{E} = (\vec{e}_1\vec{E}, \vec{e}_2\vec{E}, 0)$ in the wave frame. The last relations can be also verified for arbitrary frequencies (above the quasistatic range) by the following derivation, where the relation $V = \vec{E}\vec{h}$ is the starting point:

$$\langle VV^* \rangle = \langle\vec{E}\vec{h}(\vec{E}\vec{h})^*\rangle = \langle|\vec{E}\vec{h}|^2\rangle = \langle|\vec{E}\vec{h}_p|^2\rangle = \langle|\vec{E}|^2|\vec{h}_p|^2|\cos(\theta)|^2\rangle = \frac{1}{2}|\vec{h}_p|^2\langle|\vec{E}|^2\rangle \tag{5}$$

with $\vec{h}$ as the effective length vector that can be replaced by $\vec{h}_p$ as $\vec{e}_3\vec{E} = 0$. As we assume unpolarized waves, the angle θ between $\vec{E}$ and $\vec{h}_p$ can have all possible values, hence the time average $\langle|\cos^2(\theta)|\rangle = \frac{1}{2}$. As the received flux is the sum of the background flux and the flux from the SED signal, the background has to be subtracted, and a rearrangement of equation (2) leads to the following formula for the calculation of the incident power flux of the SEDs:

$$\langle S_{Flux}\rangle_{SED} = \langle S_{Flux}\rangle_{total} - \langle S_{Flux}\rangle_{background} = \frac{\langle V_n V_n^* \rangle_{total} - \langle V_n V_n^* \rangle_{background}}{Z_0|\vec{h}_p|^2} \tag{6}$$

The background signal intensity at each frequency channel was calculated hourly as the mean intensity of all signals after the elimination of stronger and weaker signals lying outside of $\pm 4\sigma$ (standard deviations) around the most frequent intensity.

4   Results of calculations and discussion

4.1   Projection of the effective length vector on the wave plane

Figure 3 shows the calculated magnitude of the projection of the effective length vector, $|\vec{h}_p|$, on the wave plane as a function of frequency and for those times when SED signals occur. There are some interesting points about this diagram: At the lowest frequencies $|\vec{h}_p| \approx 1.5$ m for the monopoles (at 1275 kHz) and $|\vec{h}_p| \approx 3.2$ m for the dipole (at 1825 kHz). This is close to the values for the effective length of 1.68 m for the monopole and 3.06 m for the dipole mode in the quasistatic frequency range found by Zarka et al. [2004]. The slight differences are due to the frequencies lying at the upper border of the quasistatic range, and the values given by Zarka et al. [2004] are the absolute length of the effective length vector without projection on the wave plane. Secondly, there are some points even at higher frequencies, where $|\vec{h}_p|$ is quite small, which is due to a direction of incidence close to the direction of the effective length vector leading to a small value for the projection of the effective length vector on the wave plane. On the other hand, the majority of the points form curves which can be compared quite well to the background intensity as a

function of frequency displayed in Figure 2: In the dipole mode the maximum of $|\vec{h}_p|$ has a value of 34 m at the frequency of 8.8 MHz, which is in perfect agreement with the resonance in the right panel of Figure 2, and for the monopole mode this maximum has a value of 21 m and can be found at a frequency of 9.0 MHz, which is a slight difference to the antenna resonance at 9.5 MHz as displayed in the left panel of Figure 2. Interestingly, there also appears a small peak around 7.5 MHz in the monopole mode
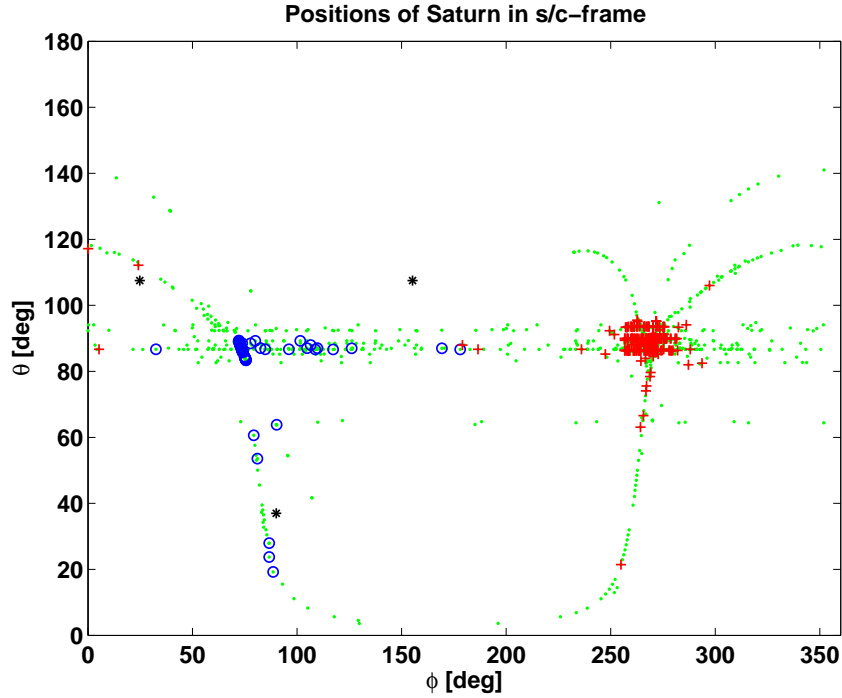

Figure 4: *Positions of Saturn in the s/c–frame at the times when SED signals occur (green dots). The black stars mark the positions of the 3 physical antennas, the red crosses and the blue circles mark the 2 different populations of $|\vec{h}_p|$ above 13.5 MHz.*

of our calculation as well as in the background measurement, but the peaks appearing around 3 MHz and 13 MHz in the monopole mode background measurements are not reproduced in our calculations. The nature of these peaks is unclear, and they cannot be explained on the basis of antenna pattern changes, so maybe they stem from some s/c internal interferences as they appear just on the monopoles which are driven against the s/c–body in contrast to the dipole. Another interesting feature of Figure 3 can be seen for frequencies above 10 MHz, where the curves in the monopole as well as in the dipole mode are split into 2 branches each. The reason for this is a geometrical one and can be seen in Figure 4: The blue circles mark those positions of Saturn, where the calculation of $|\vec{h}_p|$ leads to the lower branch of the monopole curve, and the red crosses correspond to those Saturn positions, where the higher branch of the monopole curve was calculated. It can be seen in Figure 4 that the lower branch (circles) is due to signals that stem mainly from azimuth values $\phi < 180°$, and for the higher branch (crosses) we have $\phi > 180°$ in the s/c fixed coordinate system. Azimuth values of $\phi < 180°$ (+y-hemisphere) correspond to the side of the Cassini s/c where the RPWS antenna system and the magnetometer boom

are mounted (the black stars in Figure 4 are the directions of the physical antennas), and $\phi > 180°$ (–y-hemisphere) is the opposite side (see Gurnett et al. [2004], Fischer et al. [2001], or Cecconi and Zarka [2005] for a sketch and the definition of the Cassini s/c–frame). The reason for the two branches is in fact the distortion of the power gain pattern of the respective antenna for frequencies above the antenna resonance frequency. This distortion is more pronounced for the monopole than for the dipole. Additionally it can be seen in Figure 4 that most SEDs happened when Saturn was in a position of $\theta = 90°$, which is the x–y plane of the s/c–frame, and here the most common azimuths were $\phi = 90°$ and especially $\phi = 270°$. The former is the +y-direction of the magnetometer boom, and the latter the –y-direction, which is in fact the direction in which the non–rotatable cameras of the Cassini Imaging Science Subsystem (ISS) are looking, hence the s/c is often brought into this position to take images of Saturn.
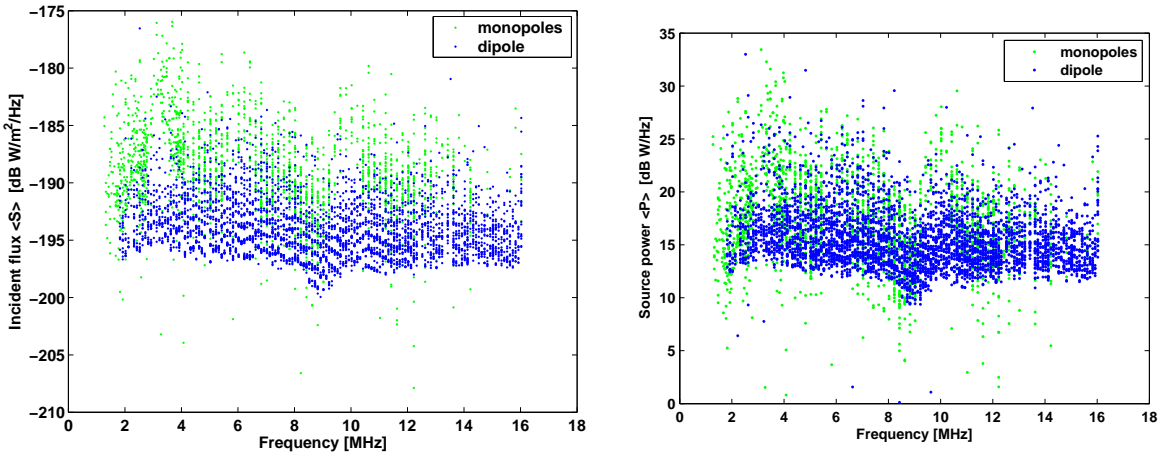

Figure 5: Left side: Incident fluxes of SED signals as a function of frequency recorded in monopole or dipole mode. Right side: Source powers (calculated from the incident flux assuming isotropic radiation) of SED signals as a function of frequency recorded in monopole or dipole mode.

4.2   Incident flux and source power as a function of frequency

Applying equation (6) we calculated the incident flux of the SEDs by subtracting the background signal from the measurement signal and dividing the result by the impedance of free space and the "reception area" $|\vec{h}_p|^2$, and this incident flux S is displayed in the left panel of Figure 5 for all recorded SEDs. It turns out that there is just a slight decrease of the incident flux for SEDs around the frequency of 2 MHz, which can be explained by a natural damping effect of Saturn's ionosphere. There is also a small decrease by 2–3 dB of the incident flux around 9 MHz, which is an artificial effect due to the imperfect modelling around the antenna resonance. The source power $\langle P \rangle_{SED}$, which is the spectral power emitted during one SED event (right panel of Figure 5), is calculated from the incident power flux $\langle S_{Flux} \rangle_{SED}$ by assuming an isotropic radiation, i.e.:

$$\langle P \rangle_{SED} = 4\pi r^2 \langle S_{Flux} \rangle_{SED} \tag{7}$$

with r as the distance between Cassini and the surface of Saturn at the time when the SED is recorded. Calculating the mean source powers at frequencies $f > 4$ MHz and fitting the results to a curve $\langle P \rangle_{SED} \sim f^{-x}$ we find a decrease of spectral power in the frequency range 4 to 16 MHz with $f^{-0.5}$, which corresponds to a fall–off by 3 dB from 4 to 16 MHz. This suggests that we are on the "rolloff" side of the spectrum at frequencies above the peak frequency with the maximum spectral power. Nevertheless the flatness still indicates that SEDs are much faster discharge than typical terrestrial lightning flashes. We also calculated the mean source powers of all SEDs occurring in the various storm systems 0, A, B, and C in 2004: We found 220 W/Hz for the storm 0 at the end of May (~ 100 flashes), 65 W/Hz for the storm A in the middle of July (~ 700 flashes), 145 W/Hz for the storm B at the beginning of August (~ 300 flashes), and 40 W/Hz for the storm C in September (~ 4200 flashes). The mean source power of all 5300 flashes found for the year 2004 is around 50 W/Hz, a value that is half of the 100 W/Hz found for the SEDs recorded by Voyager 1. We note that such a source power corresponds to a flux density of about 200 Jy at Earth orbit, hence SEDs could be detectable with special techniques by the world largest radio decameter telescope UTR–2 in the Ukraine, which has a sensitivity of a few Jy.

5   Conclusion

Complex effective antenna length vectors were calculated from a theoretical simulation of the Cassini spacecraft by a wire–grid, and they were used for the first time to calculate the incident power flux of signals from Saturnian lightning. The method worked quite well, and the true source power spectrum of the SEDs was found to have a slight decrease with $f^{-0.5}$ for the frequencies f from 4 to 16 MHz suggesting that Cassini/RPWS was sampling the "rolloff" side of the spectrum. The mean source power of all Saturn lightning flashes observed by Cassini/RPWS in 2004 was about 50 W/Hz, similar to the measurements of Voyager 1 in the early 1980s.

References

Cecconi, B., and P. Zarka, Direction finding and antenna calibration through analytical inversion of radio measurements performed using a system of 2 or 3 electric dipole wire antennas, *Radio Science*, **40**, 3, RS3003, doi:10.1029/2004RS003070, 2005.

Collin, R. E., and F. J. Zucker, Antenna Theory, Part 1, McGraw–Hill Book Compony Inc., 1969.

Desch, M. D., G. Fischer, M. L. Kaiser, W. Farrell, W. S. Kurth, D. A. Gurnett, P. Zarka, A. Lecacheux, C. Porco, A. Ingersoll, U. Dyudina, Cassini RPWS and imaging observations of Saturn lightning, in *Planetary Radio Emissions VI*, H. O. Rucker, W. S. Kurth, and G. Mann (eds.), Austrian Academy of Sciences Press, Vienna, 2006, *this issue*.

Dulk, G. A., W. C. Erickson, R. Manning, and J.-L. Bougeret, Calibration of low–frequency radio telescopes using the galactic background radiation, *Astron. Astrophys.*, **365**, 294–300, 2001.

Evans, D. R., J. H. Romig, C. W. Hord, K. E. Simmons, J. W. Warwick, and A. L. Lane, The source of Saturn electrostatic discharges, *Nature*, **299**, 236, 1982.

Fischer, G., W. Macher, H. O. Rucker, H. P. Ladreiter, D. F. Vogl, and the Cassini RPWS Team, Wire-Grid modelling of Cassini spacecraft for the determination of effective antenna length vectors of the RPWS antennas, in *Planetary Radio Emissions V*, Rucker H. O., Kaiser M. L., Leblanc Y. (eds.), Austrian Academy of Sciences Press, Vienna, 347–356, 2001.

Fischer, G., M. D. Desch, P. Zarka, M. L. Kaiser, D. A. Gurnett, W. S. Kurth, W. Macher, H. O. Rucker, A. Lecacheux, W. M. Farrell, and B. Cecconi, Saturn lightning recorded by Cassini/RPWS in 2004, *Icarus*, in press, 2006.

Gurnett, D. A., and 29 co–authors, The Cassini Radio and Plasma Wave investigation, *Space Sci. Rev.*, **114**, 1, 395–463, 2004.

Gurnett, D. A., and 26 co–authors, Radio and plasma wave observations at Saturn from Cassini's approach and first orbit, *Science*, **307**, 1255–1259, 2005.

Macher, W., Theorie effektiver Höhenvektoren von Antennen mit Anwendung auf das Radio and Plasma Wave Science Experiment der Cassini Raumsonde, Diploma Thesis at the University of Technology Graz, Austria, 1997.

Rakov, V. A., and M. A. Uman, Lightning, Physics and Effects, Cambridge Univ. Press, Cambridge, 2003.

Rucker, H. O., W. Macher, R. Manning, and H. P. Ladreiter, Cassini model rheometry, *Radio Sci.*, **31**, 6, 1299–1311, 1996.

Vogl, D. F., B. Cecconi, W. Macher, P. Zarka, H.-P. Ladreiter, P. Fedou, A. Lecacheux, T. Averkamp, G. Fischer, H. O. Rucker, D. A. Gurnett, W. S. Kurth, and G. B. Hospodarsky, In-flight calibration of the Cassini–Radio and Plasma Wave Science (RPWS) antenna system for direction-finding and polarization measurements, *J. Geophys. Res.*, **109**, A09S17, doi:10.1029/2003JA010261, July 9, 2004.

Zarka, P., and B. M. Pedersen, Statistical study of Saturn electrostatic discharges, *J. Geophys. Res.*, **88**, 9007–9018, 1983.

Zarka, P., B. Cecconi, and W. S. Kurth, Jupiter's low-frequency radio spectrum from Cassini/Radio and Plasma Wave (RPWS) absolute flux density measurements, *J. Geophys. Res.*, **109**, A09S15, doi:10.1029/2003JA010260, Aug. 14, 2004.